Mass distributions of the system ^{136}Xe + ^{208}Pb at laboratory energies around the Coulomb barrier: A candidate reaction for the production of neutron-rich nuclei at $N = 126$

E. M. Kozulin,[1] E. Vardaci,[2] G. N. Knyazheva,[1] A. A. Bogachev,[1] S. N. Dmitriev,[1] I. M. Itkis,[1] M. G. Itkis,[1] A. G. Knyazev,[1] T. A. Loktev,[1] K. V. Novikov,[1] E. A. Razinkov,[1] O. V. Rudakov,[1] S. V. Smirnov,[1] W. Trzaska,[3] and V. I. Zagrebaev[1]

[1]*Flerov Laboratory of Nuclear Reaction, Joint Institute for Nuclear Research, 141980 Dubna, Moscow region, Russia*

[2]*Dipartimento di Scienze Fisiche dell'Universitá degli Studi di Napoli "Federico II" and Istituto Nazionale di Fisica Nucleare, Sezione di Napoli, Napoli, Italy*

[3]*Department of Physics, University of Jyväskylä, Jyväskylä, Finland*

(Received 23 May 2012; revised manuscript received 13 August 2012; published 10 October 2012)

Reaction products from the system ^{136}Xe + ^{208}Pb at ^{136}Xe ions laboratory energies of 700, 870, and 1020 MeV were studied by two-body kinematics and by a catcher-foil activity analysis to explore the theoretically proposed suitability of such reaction as a means to produce neutron-rich nuclei in the neutron shell closure $N = 126$. Cross sections for products heavier than ^{208}Pb were measured and were found sensibly larger than new theoretical predictions. Transfers of up to 16 nucleons from Xe to Pb were observed.

DOI: 10.1103/PhysRevC.86.044611 PACS number(s): 25.70.Hi, 25.70.Lm

I. INTRODUCTION

The transfer of many nucleons has been pointed out in several works as a feasible route to synthesize heavy nuclei on the neuron-rich side of the stability line [1–3]. This has given rise to a renewed interest toward the physics of mass transfer processes, from few to many nucleons. In a recent review [4], it is shown experimentally that even at energies close to the Coulomb barrier the cross sections for the transfer of several protons and neutrons are relatively high.

On the basis of a novel multidimensional model [3,5,6], multinucleon transfer process, at bombarding energies close to the Coulomb barrier, has been suggested as a possible pathway to populate neutron-rich nuclei in the region of the neutron shell closure $N = 126$. This region of the nuclear map is of relevant interest for a number of reasons that cover from the alteration of the shell gap in presence of large neutron excess to the astrophysical nucleogenesis [3]. Considering the wide gap between the stability line and the predicted neutron drip-line, this region is also the most unknown and less studied one because it is not reachable with stable projectiles neither by fusion-fission nor by fusion-evaporation reactions.

The model in Ref. [3] has a multidimensional Langevin type dynamical approach and has indeed been quite successful in reproducing many recent and older data from near-barrier to above-barrier reactions [5,6] on a wide range of masses. According to this model, the reaction ^{136}Xe + ^{208}Pb at energies around the Coulomb barrier, is a good candidate for the production of new neutron-rich isotopes in the region of the neutron shell closure $N = 126$. Calculations demonstrate that the production of a few tens of unknown neutron-rich target-like fragments (TLF) in the mass region $A \approx 200$ is possible with cross sections of not less than 1 μb if the multinucleon transfer occurs. It is worth to remark that the multinucleon transfer process conjectured in [3] is more favorable with respect to the case of the cold fragmentation reaction ^{208}Pb(1A GeV) + Be [7], where nuclei in the same mass region were indeed produced, since the production cross sections in this reaction are between one and two order of magnitude less than expected in the low-energy multinucleon transfer reactions [6].

The choice of the reaction ^{136}Xe + ^{208}Pb is based on two qualifying points: 1) the stabilizing effects of the neutron closed shell $N = 82$ for ^{136}Xe and $N = 126$ for ^{208}Pb; 2) the specific trend of the Q_{gg} values of all possible mass transfer channels (Fig. 1): Q_{gg} values are close to zero for mass transfers that push the primary TLF toward symmetry and become more and more negative for TLF heavier than ^{208}Pb. The Q_{gg} distributions in Fig. 1 are computed by the following procedure: first, for each mass number of the TLF, A_{TLF}, the average atomic number of the TLF, $\langle Z_{TLF}\rangle$, is chosen so to have the charge-to-mass ratio equal to that of the compound nucleus; second, a gaussian curve is built in the range $\langle Z_{TLF}\rangle \pm 6$, and for each integer value of Z and the same A_{TLF} a Q_{gg} is calculated. The average value of all these Q_{gg}, for each A_{TLF}, is plotted in Fig. 1 as the solid thick curve; the solid thin curve in Fig. 1 refers to the maximum Q_{gg} for each A_{TLF}.

The two points mentioned above offer three important advantages. First, protons may experience a higher mobility because of the neutron closed shell in the projectile and target, and the transfer of several protons from Xe to Pb may lead to very neutron-rich nuclides, i.e., in the region of osmium and platinum [3]. A schematic guideline of such a process is shown in Fig. 2. Second, for the transfers that produce TLF with masses around 200 u or lower, the Q_{gg} are about zero, and windows of total kinetic energy lost select in turn windows of available excitation energy to the primary fragments. In this way, it is possible to gate on TLF that experience lower excitation energy.

Third, because of the large negative Q_{gg} values, TLF heavier than Pb are relatively less excited, with a consequential lower loss of neutrons or higher survival probability against fission. This last feature is very important to preserve the number of neutrons of the primary TLF and thus the ratio N/Z. This point will be addressed later in more detail.

In the above framework, the motivation of this study was to measure the mass distribution of the primary binary fragments

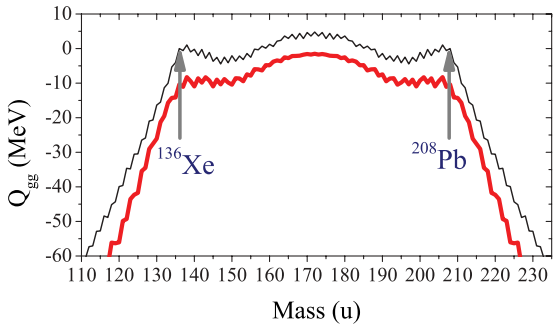

FIG. 1. (Color online) Q_{gg} distribution for all possible mass transfers. $Q_{gg} = M_P + M_T - M_{TLF} - M_{PLF}$, where M_P and M_T are the masses of the projectile and the target, and M_{TLF} and M_{PLF} are the masses of the target-like and projectile-like primary fragments, respectively. Thick line corresponds to average Q_{gg}; thin line corresponds to maximum Q_{gg} (see text for details).

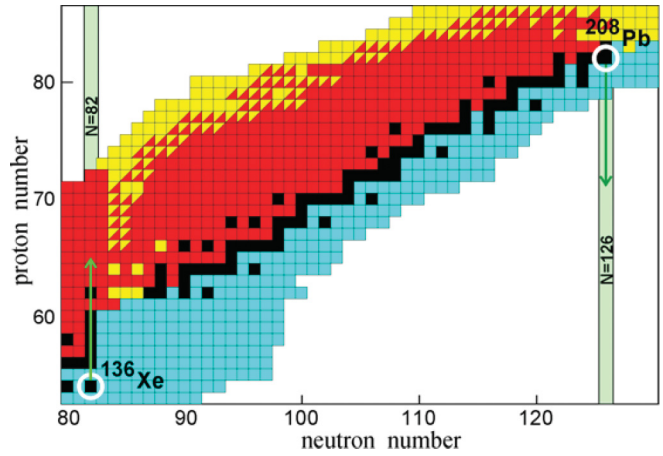

FIG. 2. (Color online) Schematic picture of proton transfer along neutron closed shell in low-energy collisions of ^{136}Xe with ^{208}Pb. Black rectangles indicate stable nuclei.

of the reaction ^{136}Xe + ^{208}Pb at energies from the Coulomb barrier up to well above it and to search for large mass transfers resulting in TLF heavier than the target. The trend of the mass distribution around mass 200 u can provide us for a reference frame to search, in a more detailed experiment, for neutron-rich nuclides in the region of osmium and platinum.

Our study was organized on two independent experimental techniques: two-body coincidence and catcher-foil activity analysis. The first one gives us the opportunity to explore the production cross section of primary TLF and to define the most convenient conditions concerning the bombarding energy for their production and survival against sequential fission. The second one allows us to have a firm identification of some α-emitter TLF (secondary fragments) and to measure their production cross sections. By combining the two methods we can have a relatively wide view of the features of the primary and secondary TLF which allow us to evaluate if such a reaction can be further studied with a more refined technique to reach the full identification of the fragments, in charge and mass. Furthermore, our study constitutes an important mean to provide new data and feedback to a model that, when extended to heavier colliding partners [6], indicates a feasible route for the production of neutron-rich superheavy elements not reachable by hot fusion reactions. These aspects made our experiment extremely worthwhile. The system ^{136}Xe + ^{208}Pb was indeed studied experimentally in the past, but with different purposes [8,9].

II. MASS-ENERGY AND ANGULAR DISTRIBUTION MEASUREMENTS OF BINARY FRAGMENTS OF THE SYSTEM ^{136}Xe + ^{208}Pb

The first experiment was carried out at the Flerov Laboratory of Nuclear Reactions at the U-400M cyclotron. A beam of 700, 870, and 1020 MeV ^{136}Xe ions struck a layer of 200 μg/cm^2 ^{208}Pb (99.9% enriched) deposited on 50 μg/cm^2 carbon backing. Beam intensity on target was 5 nA.

In the two-body coincidence method two products were detected in coincidence by the two-arm time-of-flight spectrometer CORSET [10,11]. Each arm of the spectrometer consists of a compact start detector and a position-sensitive stop detector, both based on microchannel plates. The distance between start and stop detectors was 19 cm. Start detectors were placed at a distance of 7 cm from the target. The acceptance of the spectrometer was $\pm 8^\circ$ in the reaction plane. The angular resolution of the stop detectors is 0.3 degree. The arms of the spectrometer were positioned in an optimal way according to the kinematics of the reaction. The positions of the arms of the spectrometer have been changed several times during the experiment. This arrangement allows to detect the coincident binary fragments over an angular range 25°–70° in the laboratory frame that corresponds to the center-of-mass angle range 40°–140°. The differential cross sections of the primary binary fragments were obtained after normalization

TABLE I. Energy-dependent characteristics for the reaction under study. E_{lab} and $E_{c.m.}$ are the energies in the laboratory and center-of-mass systems, respectively; $\theta_{gr}^{c.m.}$ and θ_{gr}^{lab} are the grazing angles in the laboratory and center-of-mass systems; L_{gr} is the grazing angular momentum ($\theta_{gr}^{c.m.}$ and L_{gr} were calculated using the NRV codes [12]); σ_R is the reaction cross section [14]; θ_{max}^{PLF} and θ_{max}^{TLF} are the laboratory angles for maximum yield for projectile- and target-like fragments; Seq. fiss.—the yield of TLF going to sequential fission; σ_{exp}^{d} is experimental cross section for damped events.

E_{lab}, MeV	$E_{c.m.}$, MeV	$\theta_{gr}^{c.m.}$, deg	L_{gr}, $\hbar$	σ_R, b	θ_{gr}^{lab}, deg	θ_{max}^{PLF}, deg	θ_{max}^{TLF}, deg	Seq. fiss., %	σ_{exp}^{d}, b
700 ± 14	423	148	87	0.21	110	–	–	~0	0.2 ± 0.1
870 ± 17	526	81	320	1.7	51	46 ± 2	50 ± 2	33 ± 10	1.1 ± 0.4
1020 ± 20	617	61	432	2.6	38	32 ± 2	62 ± 2	55 ± 10	1.3 ± 0.4

to elastic scattering detected by CORSET and by the current integration by means of a Faraday cup.

Primary masses, velocities, energies and angles in the center-of-mass system of reaction products were calculated from measured velocities and angles by using the momentum and energy conservation laws with the assumption that the mass of the composite system is equal to $M_{\text{target}} + M_{\text{projectile}}$. Extraction of the binary reaction channels with full momentum transfer was based on the analysis of the kinematics diagram (see [10,11] for details). The mass and energy resolutions of the present CORSET setup, which define the bin width of the experimental mass and energy yield curves, are taken as the FWHM, respectively, of the mass and energy spectra constructed for the elastic scattering. In the above conditions, the mass resolution of the spectrometer is 7 u; the energy resolution is 25 MeV.

A. Mass-energy distributions

Mass-TKE (total kinetic energy) distributions of primary binary fragments were measured in the energy range from about the Coulomb barrier ($V_C = 421.5$ MeV [12]) to well above it and are shown in Fig. 3. Table I contains other details about the reaction parameters. At a first glance, Fig. 3 suggests that besides the elastic and quasielastic components, a significant part of events has a large dissipation of the initial kinetic energy which indicates the presence of strongly damped collisions.

It is important to remark that sequential fission (the fission of the heavy TLF after the primary interaction) can pollute the true two-body coincidence events. The removal of these events

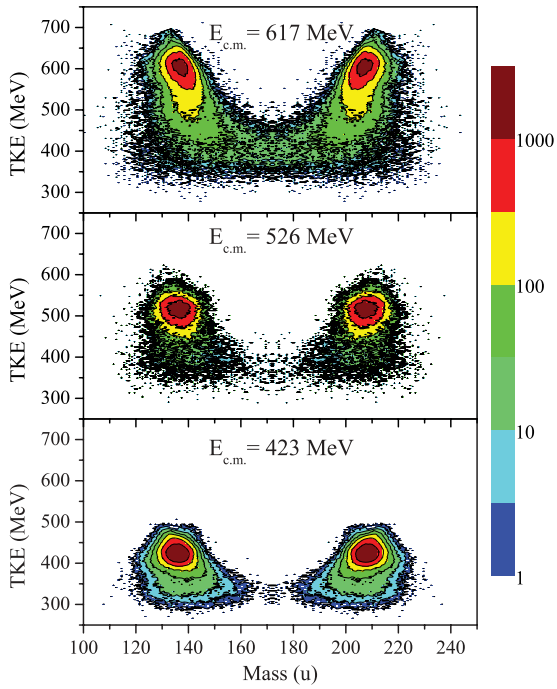

FIG. 3. (Color online) Mass-energy distributions of the primary binary fragments obtained in the reaction ^{136}Xe + ^{208}Pb at c.m. energies of 423, 526, and 617 MeV, and integrated over the angular range of 40°–140° in the c.m. Only true two-body events are included.

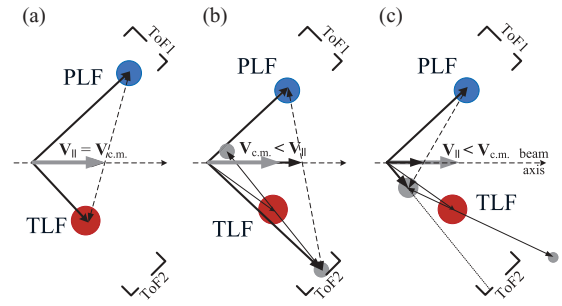

FIG. 4. (Color online) Kinematic diagrams: (a) for binary events with full momentum transfer; (b) and (c) for the case of sequential fission of TLF.

was based on the analysis of the kinematic diagram built with the velocity vectors of two detected reaction products. The method can be better understood by following the diagrams in Fig. 4.

For full momentum transfer events, the velocity $V_{\|}$ is computed event by event. For a true two-body process $V_{\|}$ should equal the center-of-mass velocity of the scissioning system $V_{\text{c.m.}}$ [cf. Fig. 4(a)]. In the case of sequential fission of the TLF, $V_{\|}$ deviates from $V_{\text{c.m.}}$ and only two cases can occur. If the detected sequential fission fragment is the one that travels forward in the reference frame of the TLF, $V_{\|}$ is larger than $V_{\text{c.m.}}$ [cf. Fig. 4(b)]; if it is the one that travels backward, then $V_{\|}$ is lower than $V_{\text{c.m.}}$ [cf. Fig. 4(c)].

The distribution of the $V_{\perp}$ component of fragment velocity (projection of the fragment velocity vector onto the plane perpendicular to the beam axis [10]) is expected to be around zero. Figure 5 illustrates the distribution of $V_{\|}$ and $V_{\perp}$ for the reaction ^{136}Xe + ^{208}Pb at a beam energy of 1020 MeV, obtained from the measured velocity vectors. This figure makes clear that the spectrometer detects three main groups of events. The events for which $V_{\|}$ is equal to $V_{\text{c.m.}}$ (within the contour line) correspond to the binary reaction products [cf. Fig. 4(a)], while the groups of events with $V_{\|}$ lower [cf. Fig. 4(b)] and higher [cf. Fig. 4(c)] than $V_{\text{c.m.}}$ correspond to sequential fission of excited target-like fragments. Therefore, in Fig. 3 and in the following analysis only the two-body events inside the circle are used.

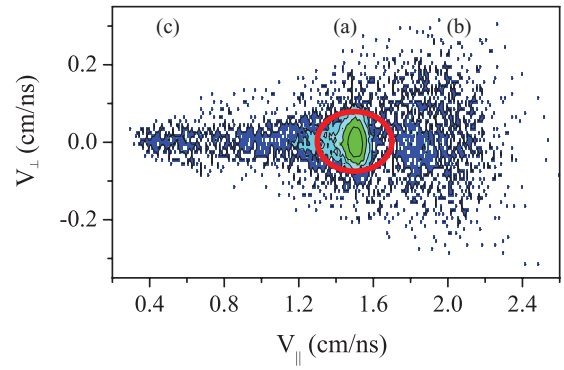

FIG. 5. (Color online) Distribution of velocity components $V_{\|}$ and $V_{\perp}$ for the reaction ^{136}Xe + ^{208}Pb at a beam energy of 1020 MeV and a position of the ToF arms of 45° and −45°; the circle limits the true two-body reaction site.

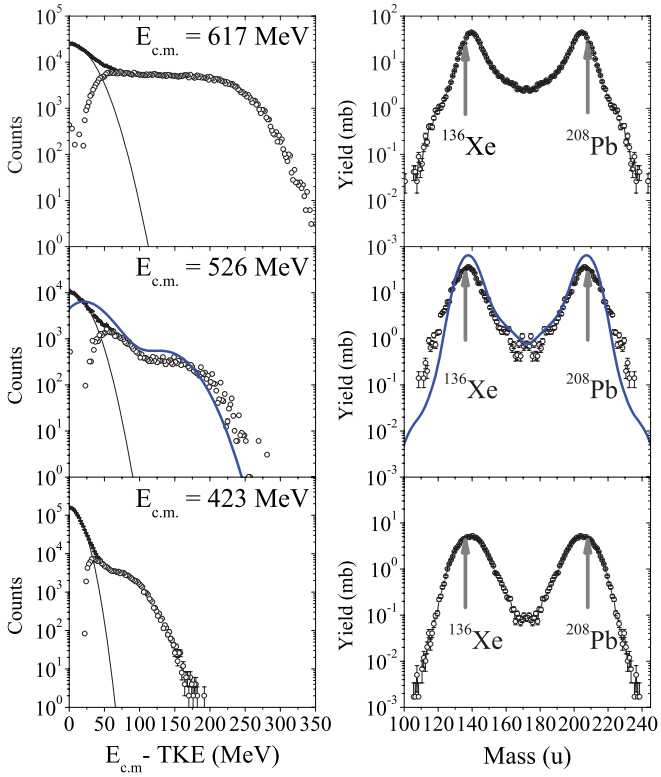

FIG. 6. (Color online) Left panel: TKEL distributions of the ^{136}Xe + ^{208}Pb reactions for the c.m. energies of 423, 526, and 617 MeV. The thin lines are the elastic and quasielastic (Gaussian-like) contributions; open circles are the difference between experimental and the Gaussian distributions. Right panel: open circles are the primary mass distributions of damped collisions for binary events with energy losses greater than 40 MeV at the c.m. energies of 423, 526, and 617 MeV. For the case at 526 MeV the thick solid lines represent new calculations with the model in Ref. [3], convoluted with the experimental resolution.

The relative contribution of sequential fission to the full set of coincidences detected amounts to $55 \pm 10\%$ at incident energy of 1020 MeV, $33 \pm 10\%$ at 870 MeV, and less than 5% at 700 MeV. As expected, the contribution of sequential fission increases with the bombarding energy confirming that the better conditions to benefit of the survival of the TLF is to be close enough to the Coulomb barrier.

The distributions of the total kinetic energy lost TKEL ($=E_{\text{c.m.}} - \text{TKE}$) for all detected events are shown in Fig. 6 (left panel). These distributions give the extent of energy dissipation with increasing bombarding energy. Lower TKEL values correspond to quasielastic processes; higher TKEL values correspond to more damped events. If we use a Gaussian curve to reasonably take into account the quasielastic component we observe that most of the damped events are localized at TKEL values above 40 MeV. Furthermore, TKEL increases with the bombarding energy: at 423 MeV the maximum value of dissipated energy is about 200 MeV, at 617 is 350 MeV. For the case at 526 MeV new calculations, with the model in Ref. [3], of TKEL distribution with energy losses greater than 10 MeV is also presented in Fig. 6. The calculated yield curve is convoluted with the experimental energy resolution. The calculation reproduces qualitatively the trend of the experimental distribution, but underestimates the maximum amount of dissipated energy.

Because of the trend of the Q_{gg} distribution, TKEL equals, to a good degree, the excitation energy $E^*_{\text{f}} = \text{TKEL} + Q_{\text{gg}}$ available for both primary fragments, at least for fragments with mass between Xe and Pb. Considering the distribution of events with TKEL > 40 MeV and setting $Q_{\text{gg}} = 0$, the average excitation energies are about 50 MeV, 70 MeV, and 120 MeV at center-of-mass energies of 423, 526, and 617 MeV, respectively.

The mass distributions of the primary fragments with TKEL > 40 MeV are shown in the right panel of Fig. 6. Due to such selection of TKEL, most of the quasielastic events have been removed. At all measured energies the mass distribution has a two-humped shape. The yield of the fragments in the mass region 136 ± 8 u is more than 60% of all damped events at all measured energies. Furthermore, we observe fragments with mass up to 238 with cross section of the order of 0.1 mb in the reaction at $E_{\text{c.m.}} = 526$ MeV. Considering the mass resolution of the CORSET spectrometer, this remarkably means that a net mass transfer from projectile to target of about 20 nucleons occurs in this reaction.

For the case at 526 MeV the theoretical primary mass distribution is given. Also in this case, the calculated yield curve has been convoluted with the experimental mass resolution. One can see a good agreement between theoretical and experimental yields only in the nearly symmetric region. Indeed, the artificial normalization of the calculated yield curve, by a factor of about 0.4, reveals that the shape of the experimental curve can be very well reproduced in the full mass range except for the superasymmetric region, where the underestimation will increase even more. This kind of normalization problem are quite frequent and this result constitute a feedback for the present model. This allows us to conclude that the model is, roughly within a factor two, in good agreement with the experimental data in the region where Q_{gg} is nearly zero (the region of major interest for this work) but underestimates by a large extent the primary mass distribution in the superasymmetric fragment mass region. Clearly, the lack of knowledge of the atomic number distribution in this mass region is an unwanted drawback, but this result may give impulse for a more detailed experimental work with respect to the present exploration of the features of the reaction products.

Additional characteristic features of the reaction under study come from the following considerations about the survival probability of the primary fragments. All fragments in Fig. 6 are considerably excited and de-excite by neutron evaporation (sequential fission has been removed). Since we are also interested in the production cross section of the secondary fragments (namely, primary fragments after neutron evaporation), we can provide at this stage a first estimate of such cross section by correcting the primary mass distribution for neutron emission assuming that the available excitation energy E^*_{f} is divided between the two primary fragments according to their mass ratio [15] and each neutron takes away on the average 10 MeV (sum of binding energy of one neutron and its kinetic energy). For the values of Q_{gg} the average value distribution was used (see Fig. 1).

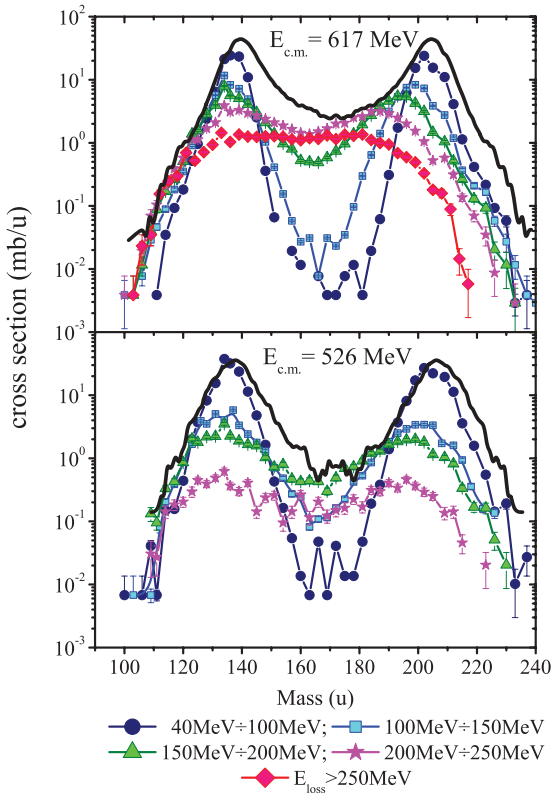

FIG. 7. (Color online) Mass distributions corrected for neutron emission for different windows of TKEL (see text). The average values of Q_{gg} are used. Full solid line is the primary distribution for all TKEL.

These mass distributions have a lot of interesting features. With increasing TKEL (namely, more excitation energy available to primary fragments), more neutrons are evaporated. Hence, TLF and PLF masses drift toward lower masses, respectively. However, TLF drift at a faster rate than PLF because the mechanism (arbitrarily chosen) to split the excitation energy awards more energy to the heavier fragment. It is important to remark that the mass drift in Fig. 7 is an artificial effect, though plausible, which comes from the attempt to reconstruct the secondary fragment mass distributions from the primary ones. In the cases of TLF heavier than Pb, a large (negative) Q_{gg} would reduce even more the available excitation energy and fewer neutrons would be evaporated. Consequently, the rate of mass drift would be slower for such heavy fragments. This means that larger mass transfers from projectile to target, being characterized by larger negative Q_{gg} values, end up in a larger survival probability against neutron evaporation. This case is particularly important for mass transfer from Xe to Pb where larger negative Q_{gg} contribute to further reduce the excitation energy.

According to Fig. 7, the contribution of the heavy secondary fragments with masses around 200 u and greater than 220 u is relatively large for the lowest values of TKEL, and is larger at $E_{c.m.} = 526$ MeV. This is another important features of this reaction: not only large mass transfers can occur from projectile to target in the regime of the lower excitation energy, but also a high survival probability of these heavy TLF against the evaporation of neutrons is guaranteed by a large negative Q value. This conclusion means that the largest the mass transfer, the highest the survival probability against neutron evaporation. This feature is highly desirable if a nuclear reaction is to be chosen as a candidate reaction to produce neutron-rich nuclei.

B. Angular distributions

Other important features about the reaction mechanisms come from the angular distribution. Figure 8 shows the PLF and TLF angular distributions of the damped events and for the range of TLF masses between 200 and 216 u. At the laboratory energies of 870 and 1020 MeV the cross sections show a sharp peak around angles slightly smaller than the calculated grazing angles (see Table I). At 700 MeV (close to the Coulomb barrier) there is no peak in the angular range of our detector setup. Such behavior of the angular distributions is typical of deep inelastic scattering between heavy partners.

The cross sections σ^{d}_{exp} of the damped events were deduced by integrating these angular distributions. The results are presented in Table I. The values of σ^{d}_{exp} are smaller than total reaction cross section σ_R, except for the lowest bombarding energy. We expect this result because σ_R includes also the quasielastic and the sequential fission components.

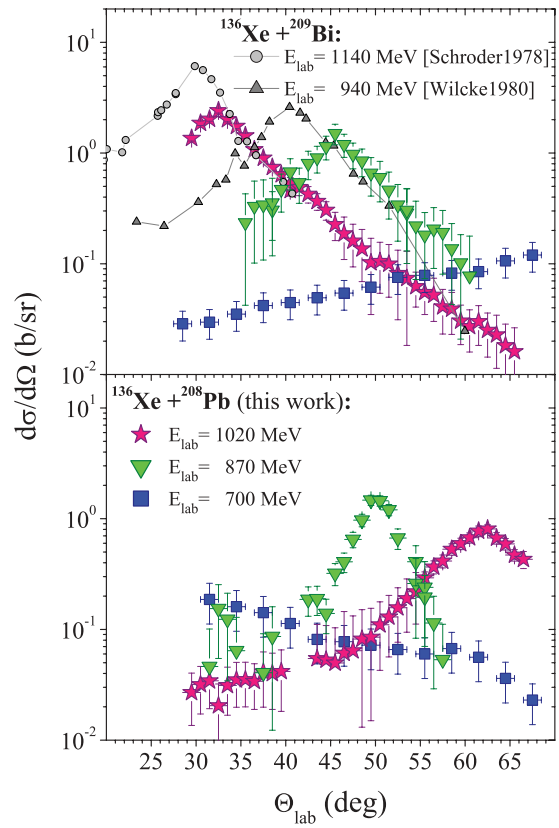

FIG. 8. (Color online) Top panel: laboratory angular distributions of the Xe-like reaction products (Wilcke1980 [14]; Schroder1978 [16]); Bottom panel: laboratory angular distributions of the Pb-like reaction products for the mass region 200–216 u.

The angular distributions of the Xe-like fragments obtained in a similar reaction ^{136}Xe + ^{209}Bi at Xe-ions energies of 940 and 1140 MeV from [14,16] are shown in the top panel of Fig. 8 for comparison. Similarly to the present experiment at energies of 870 and 1020 MeV, the cross sections peak around angles slightly more forward than the grazing angles.

The maximum production cross section of heavy nuclei occurs at $E_{\rm lab} = 870$ MeV at the laboratory angle around 50°. At the highest energy of 1020 MeV the angular distribution is however wider (FWHM is about 10° versus 4° at $E_{\rm lab} =$ 870 MeV) and the maximum cross section is lower than the cross section at $E_{\rm lab} = 870$ MeV. Considering, furthermore, that at $E_{\rm lab} = 870$ MeV the angular distribution is more focused and the heavy fragments are, on the average, 50 MeV less excited with respect to the case at $E_{\rm lab} = 1020$ MeV, the reaction ^{136}Xe + ^{208}Pb at $E_{\rm lab} = 870$ MeV seems more suitable for the search of heavy-neutron rich isotopes.

III. THE PRODUCTION CROSS SECTIONS OF α-EMITTERS NUCLEI

To provide a firm identification of some TLF with mass greater than 210 u and also to reject any artifact due to the limited resolution of the CORSET setup, we performed a second experiment on the same system at the bombarding energy of 850 MeV by using a catcher-foil activity analysis. Since the major part of nuclides with masses larger than 210 u undergoes α-decay, a careful analysis of the α-decay spectra from nuclides implanted in a catcher-foil can indeed allow us to reconstruct the cross section of the α-emitter isotopes produced in the reaction. This method also calls for a more direct comparison of the cross sections with the expectations of the model.

The experiment took place at the U-400M cyclotron. A beam of 850 MeV ^{136}Xe struck a 0.7 mg/cm^2 foil of ^{208}PbS$_4$ (99.9% enriched) deposited on 2.1 μm titanium backing. Beam intensity on target was 10 nA.

The aluminum catcher-foils covered the angles between 45° and 55° with respect to the beam, namely, the angles where the cross section for TLF has the maximum value. The TLF are implanted into the foil at the depth of about 1 μm and the α-particles from the decay of these fragments loose about 150 keV passing through the foil. The catcher-foils were irradiated for 3 d. After irradiation, the catcher-foils were removed from the chamber and α-particles were detected for 11 d. The energy resolution of the silicon detectors was 40 KeV (FWHM).

During target irradiation with beam, α-emitter nuclei are produced directly in the reaction and can also be a result of some mother nuclei decay. Thus, the amount of nucleus N_k, where k is a number in the decay chain ($k = 0$ corresponds to the mother nucleus) may be calculated [17] as

$$N_k(t) = \frac{1-e^{-\lambda_k t}}{\lambda_k}\sum_{i=0}^{k} N_i^0 - \sum_{i=0}^{k} \times \left[\prod_{j=i+1}^{k-1}\lambda_j \sum_{j=0}^{i} N_j^0 \sum_{j=i}^{k} \frac{e^{-\lambda_j t}}{\prod_{l=i,l\neq j}^{k}(\lambda_l-\lambda_j)}\right], \quad (1)$$

were N_i^0, λ_i are, respectively, the production rate and the decay probability per unit time of the nucleus i.

According to Eq. (1) the amount of radioactive nuclei is saturated for the period $3T_{1/2}$. So, only long-lived nuclei can accumulate into the foils.

After stopping the beam, the fragments are not produced in the reaction directly, but the daughter nuclei may accumulate. In this case the amount of k-th nucleus as a function of time after stopping the beam is

$$N_k(t) = N_k^1 e^{-\lambda_k t} + \sum_{i=0}^{k-1}\left[N_i^1 \prod_{j=i}^{k-1}\lambda_j \sum_{j=i}^{k} \frac{e^{-\lambda_j t}}{\prod_{l=i,l\neq j}^{k}(\lambda_l-\lambda_j)}\right], \quad (2)$$

N_k^1 is a number of kth nucleus at the end of the irradiation, calculated with Eq. (1) at time t.

Thus, the number of decay of kth nucleus during period $t_0 - t_1$ is

$$\int_{t_0}^{t_1}\lambda_k N_k(t)dt = N_k^1(e^{-\lambda_k t_0} - e^{-\lambda_k t_1}) + \lambda_k \sum_{i=0}^{k-1}\left[N_i^1 \prod_{j=i}^{k-1}\lambda_j \sum_{j=i}^{k} \frac{e^{-\lambda_j t_0} - e^{-\lambda_j t_1}}{\lambda_j \prod_{l=i,l\neq j}^{k}(\lambda_l-\lambda_j)}\right]. \quad (3)$$

The measured α-particles energy spectra are shown in the Fig. 9. The background spectrum was measured in the same conditions and for foils identical to the irradiated ones, and was taken into account. Most of the events were located between 5 and 9 MeV. The α-particle energies from the decay of Xe-like nuclei are less than 4 MeV and only nuclei with $Z > 68$ may give a contribution to energies larger than 4 MeV in the α-particle energy spectra [18].

Due to the high density of lines between 4 and 10 MeV and the relatively poor statistics a unique identification of all peaks is not possible. Since the most part of heavy nuclei following

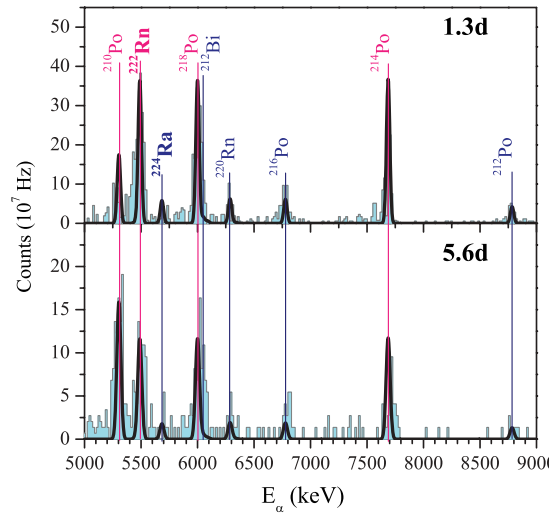

FIG. 9. (Color online) Offline α spectra 1.3 and 5.6 d after irradiation. The accumulation times were 76 and 127 h, respectively.

α-decay have the half-life from μs up to several minutes, they are not accumulated in the foils in a reasonable quantity during irradiation. Only long-lived nuclei and their daughters may be observed. These are the possible chains:

$$1)\,^{225}\mathrm{Ra} \xrightarrow[14.9\,\mathrm{d}]{\beta} {}^{225}\mathrm{Ac} \xrightarrow[10\,\mathrm{d}]{\alpha} {}^{221}\mathrm{Fr} \xrightarrow[4.9\,\mathrm{min}]{\alpha} {}^{217}\mathrm{At} \xrightarrow[32.3\,\mathrm{ms}]{\alpha}$$
$$^{213}\mathrm{Bi} \xrightarrow[45.59\,\mathrm{min}]{\beta} {}^{213}\mathrm{Po} \xrightarrow[4.2\,\mu\mathrm{s}]{\beta} {}^{209}\mathrm{Pb} \xrightarrow[3.25\,\mathrm{h}]{\beta} {}^{209}\mathrm{Bi(st)};$$
$$2)\,^{224}\mathrm{Ra} \xrightarrow[3.66\,\mathrm{d}]{\alpha} {}^{220}\mathrm{Rn} \xrightarrow[55.6\,\mathrm{s}]{\alpha} {}^{216}\mathrm{Po} \xrightarrow[145\,\mathrm{ms}]{\alpha} {}^{212}\mathrm{Pb} \xrightarrow[10.64\,\mathrm{h}]{\beta}$$
$$^{212}\mathrm{Bi} \xrightarrow[1.01\,\mathrm{h}]{\beta} {}^{212}\mathrm{Po} \xrightarrow[299\,\mathrm{ns}]{\alpha} {}^{208}\mathrm{Pb(st)};$$
$$\xrightarrow[1.01\,\mathrm{h}]{\alpha} {}^{208}\mathrm{Tl} \xrightarrow[3.05\,\mathrm{min}]{\beta} {}^{208}\mathrm{Pb(st)};$$
$$3)\,^{223}\mathrm{Ra} \xrightarrow[11.43\,\mathrm{d}]{\alpha} {}^{219}\mathrm{Rn} \xrightarrow[3.96\,\mathrm{s}]{\alpha} {}^{215}\mathrm{Po} \xrightarrow[1.781\,\mathrm{ms}]{\alpha} {}^{211}\mathrm{Pb} \xrightarrow[36.1\,\mathrm{min}]{\beta}$$
$$^{211}\mathrm{Bi} \xrightarrow[2.1\,\mathrm{min}]{\alpha} {}^{207}\mathrm{Tl} \xrightarrow[4.77\,\mathrm{min}]{\beta} {}^{207}\mathrm{Pb(st)};$$
$$4)\,^{222}\mathrm{Rn} \xrightarrow[3.82\,\mathrm{d}]{\alpha} {}^{218}\mathrm{Po} \xrightarrow[3.10\,\mathrm{min}]{\alpha} {}^{214}\mathrm{Pb} \xrightarrow[26.8\,\mathrm{min}]{\beta} {}^{214}\mathrm{Bi} \xrightarrow[19.9\,\mathrm{min}]{\beta}$$
$$^{214}\mathrm{Po} \xrightarrow[164.3\,\mu\mathrm{s}]{\alpha} {}^{210}\mathrm{Pb} \xrightarrow[22.3\,\mathrm{yr}]{\beta} {}^{210}\mathrm{Bi} \xrightarrow[5.01\,\mathrm{d}]{\beta}$$
$$^{210}\mathrm{Po} \xrightarrow[138.38\,\mathrm{d}]{\alpha} {}^{206}\mathrm{Pb(st)}.$$

The time intervals of activity measurements allow to detect only α particles from the chains of ^{224}Ra and ^{222}Rn. All α-lines of these chains have been identified in the experimental spectra.

In the fitting procedure of the growth and decay equations to the spectra in Fig. 9 only nuclei with a half-life larger than several minutes play a role. Therefore, the production cross sections may be estimated with reasonable accuracy only for these nuclei. The thick Gaussian curves in Fig. 9 are the result of the fitting procedure with the Eqs. (1) and (3). One can see that a good agreement with measured spectra is found. The cross section of 200 ± 100 μb, 17 ± 14 μb, and 2.5 ± 2 μb were obtained, respectively, for ^{210}Po, ^{222}Rn, and ^{224}Ra nuclides.

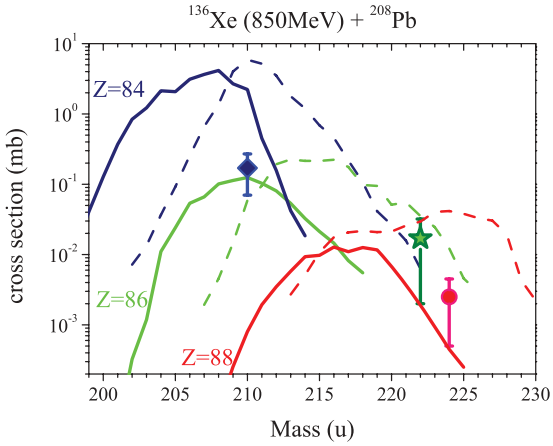

FIG. 10. (Color online) The calculated production cross section for primary (dash lines) and survived (solid lines) isotopes of Po, Rn, and Ra. The points correspond to the estimated experimental cross sections for ^{210}Po (diamond), ^{222}Rn (star), and ^{224}Ra (circle).

In Fig. 10 these values are compared to the new calculation of the model in Ref. [3]. For ^{210}Po the experimental cross section is overestimated by one order of magnitude; contrarily, the cross section of ^{222}Rn and ^{224}Ra are underestimated by about one order of magnitude, even though at the limit of the experimental error. Both results are quite unexpected because the model is known to well reproduce cross section for transfer of few nucleons; the same trend as for ^{222}Rn and ^{224}Ra in Fig. 10 was indeed recently observed in the reaction ^{160}Gd + ^{186}W at $E_{\mathrm{c.m.}} = 461.9$ MeV [19] for the transtarget reaction products near $Z = 79$.

IV. SUMMARY AND CONCLUSION

In this study of the reaction ^{136}Xe + ^{208}Pb, at energies around the Coulomb barrier, we have measured the mass and energy distributions of the two-body fragments to search for signatures of mass transfers which would produce TLF with mass around 200 u and larger than Pb with a high survival probability against fission and neutron evaporation. We have pointed out that this reaction has same specific and advantageous features that make it a suitable candidate for searching for more extreme mass transfers, like a transfer of six protons from Pb to Xe, which lead to an unexplored region of nuclei around $N = 126$, not reachable by other means.

The mass distribution of the secondary TLF reveals a broad peak around mass 200 and a long tail that extends up to almost 240 mass units for the lowest window of TKEL. This broad peak covers a cross section of several tens of mb. The long tail reaches values up to 0.1 mb. It has also been shown that the bombarding energy closer to the Coulomb barrier results in a higher survival probability against fission and neutron evaporation along with the fact that the experimental method is very effective in sorting out the sequential fission component in the mass distributions.

We do not have evidence that the large proton transfer suggested in Ref. [3] (cf. Fig. 2) occurs indeed and, at the same time, we cannot rule this process out. Charge identification is necessary to investigate on this point. However, we register a cross section around mass 200 that is sufficiently high to support the design of an experiment which combines the simultaneous identification of the mass and charge of the fragments to search for this kind of proton transfer.

Yet, the direct measurement of reaction product through their α activity confirms that a mass transfer up to 16 nucleons can occur with a cross section of the order of 200 μb for the lower mass transfer and few μb for the larger mass transfers. These cross sections are certainly of the order of magnitude that make a more detailed search for neutron-rich nuclei accessible with this reaction.

ACKNOWLEDGMENTS

The authors would like to express their gratitude to the staff of the U400M cyclotron. This work was supported by the Russian Foundation for basic Research (Grant No. 11-02-01507-a).

[1] V. V. Volkov, Phys. Rep. **44**, 93 (1978).
[2] C. H. Dasso, G. Pollarolo, and A. Winther, Phys. Rev. Lett. **73**, 1907 (1994).
[3] V. Zagrebaev and W. Greiner, Phys. Rev. Lett. **101**, 122701 (2008).
[4] L. Corradi, G. Pollarolo, and S. Szilner, J. Phys. G **36**, 113101 (2009).
[5] V. Zagrebaev and W. Greiner, J. Phys. G: Nucl. Part. Phys. **31**, 825 (2005).
[6] V. I. Zagrebaev and W. Greiner, Phys. Rev. C **83**, 044618 (2011).
[7] T. Kurtukian-Nieto, Ph.D. thesis, Santiago de Compostela, (2007).
[8] R. Vandenbosch *et al*., Nucl. Phys. A **269**, 210 (1976).
[9] H. Essel *et al*., Z. Phys. A **289**, 265 (1979).
[10] E. M. Kozulin *et al*., Instrum. Exp. Tech. **51**, 44 (2008).
[11] I. M. Itkis *et al*., Phys. Rev. C **83**, 064613 (2011).
[12] V. I. Zagrebaev *et al*., http://nrv.jinr.ru.
[13] M. G. Itkis and A. Ya. Russanov, Fiz. Elem. Chastits At. Yadra **29**, 389 (1998) [Phys. Part. Nucl. **29**, 160 (1998)].
[14] W. W. Wilcke *et al*., Phys. Rev. C **22**, 128 (1980).
[15] J. Wilczynski and H. W. Wilschut, Phys. Rev. C **39**, 2475 (1989).
[16] W. U. Schröder *et al*., Phys. Rep. C **45**, 301 (1978).
[17] E. Rutherford and F. Soddy, Phil. Mag. S. 6 **5**, 576 (1903).
[18] http://www.nndc.bnl.gov.
[19] W. Loveland, A. M. Vinodkumar, D. Peterson, and J. P. Greene, Phys. Rev. C **83**, 044610 (2011).